npj | precision oncology

Article

Published in partnership with The Hormel Institute, University of Minnesota

https://doi.org/10.1038/s41698-025-00930-9

Hepatocellular carcinoma cells downregulate PGAM2 via SIRT2-mediated deacetylation modification to enhance aerobic glycolysis

Zexuan Wang[1,2,7], Yaoyu Guo[1,2,7], Kefei Hu[1,2], Tingjiang He[1], Tong Qin[3], Ludan Zhang[1], Fang Xu[1], Yuanzhi Xu[4], Mingjiao Cheng[1,2], Jintao Zhang[1,5,6] ✉ & Qianwei Zhao[1] ✉

Phosphoglycerate mutase 2 (PGAM2) is a crucial glycolytic enzyme. Recently, we have found that both the protein and acetylation levels of PGAM2 are down-regulated in hepatocellular carcinoma (HCC) tissues. However, the functional significance of PGAM2 in HCC progression remains poorly characterized. In this study, we demonstrated that PGAM2 functioned as a tumor suppressor in HCC progression, and knockdown of PGAM2 promoted proliferation of HCC cells and tumor growth both in vitro and in vivo. Moreover, we identified lysine 100 (K100) in PGAM2 as the predominant deacetylation site of sirtuin-2 (SIRT2), and that deacetylation of K100 destabilized PGAM2 by promoting its ubiquitination and degradation. Importantly, we discovered that PGAM2 suppressed aerobic glycolysis through an enzymatic activity-independent mechanism in HCC cells. Mechanistic investigations revealed that PGAM2 knockdown upregulated lactate dehydrogenase A (LDHA) expression via activation of the signal transducer and activator of transcription 3 (STAT3). Furthermore, we found that knockdown of PGAM2 sensitized HCC cells to sorafenib treatment. In conclusion, these findings elucidate the tumor-suppressive role of PGAM2 in HCC progression and its post-translational regulation through SIRT2-mediated deacetylation, which provide novel biomarkers and therapeutic targets for HCC treatment.

According to the latest Global Cancer Statistics, as many as 830,000 liver cancer-associated mortalities were reported in 2020, making it the third most lethal cancer[1,2]. Hepatocellular carcinoma (HCC) is the predominant type of primary liver cancer, which accounts for approximately 90% of all cases[3,4]. Despite substantial research efforts to combat HCC, the drivers for HCC progression remain poorly characterized. Therefore, a more in-depth understanding of the molecular mechanisms underlying HCC progression is urgently needed to improve its diagnosis and treatment.

Phosphoglycerate mutase 2 (PGAM2) is a key glycolytic enzyme that catalyzes the conversion of 3-phosphoglycerate (3-PG) to 2-phosphoglycerate (2-PG). PGAM2 is highly expressed in muscle tissues, where it drives glycolysis and cellular energy production[5,6]. Beyond the metabolic role, emerging evidence implicates PGAM2 in regulating aerobic glycolysis and apoptosis of cancer cells through protein-protein interactions[7,8]. Notably, studies have identified *PGAM2* as a phase IV-specific gene in HCC progression while clinical correlation analysis showed that elevated nuclear PGAM2 expression predicts poorer overall survival in HCC patients[9,10]. However, the exact role of PGAM2 in the progression of HCC remains elusive.

Lysine acetylation is an evolutionarily conserved post-translational modification (PTM) that is reversibly regulated by acetyltransferases and deacetylases. Acetylation and deacetylation modifications of non-histone proteins primarily regulate the enzymatic activity, protein stability,

[1]Henan Institute of Medical and Pharmaceutical Sciences, Zhengzhou University, Zhengzhou, China. [2]BGI College, Zhengzhou University, Zhengzhou, China. [3]School of Bioengineering, Sichuan University of Science & Engineering, Yibin, China. [4]The First Affiliated Hospital of Zhengzhou University, Zhengzhou, China. [5]Henan Key Medical Laboratory of Tumor Molecular Biomarkers, Zhengzhou University, Zhengzhou, China. [6]Henan Key Laboratory of Tumor Epidemiology and National Key Laboratory of Metabolism Disorder and Esophageal Cancer Prevention & Treatment, Zhengzhou University, Zhengzhou, China. [7]These authors contributed equally: Zexuan Wang, Yaoyu Guo.
✉e-mail: jtzhang@zzu.edu.cn; qianwzhao@zzu.edu.cn

subcellular localization, and interaction networks[11–14]. Previously, we have found that the acetylation level of K100 site in PGAM2 was significantly reduced in HCC tissues[15]. This finding aligns with broader evidence that the stability and catalytic efficiency of PGAM2 function are dynamically regulated through PTMs including phosphorylation, acetylation, ubiquitination, and sumoylation[16–19]. Taken together, these findings underscore the biological significance of PTMs in regulating PGAM2 function and expression.

In this study, we explored the functional significance and regulatory mechanisms of PGAM2 in HCC progression. Our findings reveal that the deacetylase sirtuin-2 (SIRT2)-mediated deacetylation of PGAM2 at lysine 100 (K100) enhances its ubiquitination, thereby promoting degradation of PGAM2. Knockdown of PGAM2 increases the aerobic glycolysis and proliferation abilities of HCC cells via activation of the STAT3/LDHA axis. Furthermore, knockdown of PGAM2 enhances sorafenib sensitivity, while inhibition of SIRT2 attenuated acquired resistance to sorafenib in HCC cells. Collectively, our study reveals that SIRT2-mediated deacetylation of PGAM2 plays a pivotal role in the development of HCC, which provides promising biomarkers and strategies for the treatment of HCC.

Results

PGAM2 inhibits proliferation and tumor growth of HCC cells both in vitro and in vivo

To examine the function of PGAM2 in the proliferation of HCC cells, we first detected PGAM2 expression in HCC cell lines. Results showed that the PGAM2 expression was higher in SNU449 and HepG2 cell lines compared to that in HCCLM3 and Huh7 cell lines (Fig. 1A). Then we successfully established PGAM2 overexpression models in HCCLM3 and Huh7 cell lines via lentiviral infection, which was confirmed by RT-qPCR and western blot (Fig. 1B). Results revealed that overexpression of PGAM2 notably inhibited the cell viability of HCC cells (Fig. 1C, D), as well as the colony formation ability (Fig. 1E). Additionally, we knocked down PGAM2 in SNU449 and HepG2 cell lines using specific shRNAs (Fig. 1F–H). CCK-8 and colony formation assays demonstrated that knockdown of PGAM2 lead to a significant increase in the cell proliferation rate and number of colonies (Fig. 1I–K). To further explore the impact of PGAM2 knockdown on HCC development in vivo, we conducted the tumorigenicity analysis by subcutaneously injecting PGAM2 knockdown cells and controls into nude mice. Three weeks later, the mice were sacrificed and the tumors were collected for analysis (Fig. 1L). Tumors derived from PGAM2 knockdown cells exhibited a marked increase in both weight and volume compared to those from controls (Fig. 1M, N), indicating that depletion of PGAM2 promoted HCC growth in vivo. Collectively, these data suggest that PGAM2 functions as a tumor suppressor, and its down-regulation promotes HCC progression.

Deacetylation of PGAM2 at K100 site reduces its stability

To investigate the mechanism underlying down-regulation of PGAM2 in HCC tissues, we detected the stability of PGAM2 in HCC cell lines. Results showed that PGAM2 was primarily degraded by the ubiquitin-proteasome system (Fig. 2A–C). Given that acetylation modification have been reported to affect the ubiquitination and degradation of proteins, and our previous finding that the acetylation level of PGAM2 at K100 site was significantly down-regulated in HCC tissues[15], we constructed K100 deacetylation-mimic (PGAM2-K100R) and wild-type (PGAM2-WT) expressing cell lines to investigate that whether deacetylation of K100 affects the stability of PGAM2 (Fig. 2D). Compared with PGAM2-WT, PGAM2-K100R showed markedly reduced acetylation level and half-life (Fig. 2E–G). Besides, we transfected PGAM2-WT or PGAM2-K100R, along with ubiquitin-expressing plasmid into HEK293T cells, and found that the ubiquitination level of PGAM2-K100R was much higher than that of PGAM2-WT (Fig. 2H). Subsequently, we demonstrated that PGAM2-K100R expressing cells obtained higher proliferation rate and more colonies compared to those of PGAM2-WT expressing cells (Fig. 2I, J). Taken together, these data indicate that deacetylation of PGAM2 at K100 promotes its ubiquitination and degradation.

SIRT2 mediates deacetylation modification of PGAM2

It has been reported that the deacetylase SIRT2 accounts for PGAM2 deacetylation[16,17]. Here we explored whether SIRT2 could promote the degradation of PGAM2 by inducing its deacetylation at K100 site. Results showed that SIRT2 interacted with PGAM2 in cells and inhibition of the type III HDAC family (Sirtuins) with NAM increased the acetylation level of PGAM2 (Fig. 3A, B). Besides, we co-transfected plasmids expressing PGAM2-WT or PGAM2-K100R, along with SIRT2 or control in HEK293T cells. We found that the acetylation level of PGAM2-WT was significantly reduced upon SIRT2 overexpression. However, SIRT2 had little impact on the acetylation level of PGAM2-K100R (Fig. 3C), suggesting that K100 was the main deacetylation site of PGAM2 regulated by SIRT2. Moreover, proteins interaction analysis predicted that the deacetylase domain of SIRT2 interacted with the N-domain of PGAM2, including the sites surrounding K100 (Fig. 3D, E). It is highly possible that acetylation of K100 in PGAM2 affected the affinity and interaction between PGAM2 and SIRT2. In support of this notion, we detected the affinities between SIRT2 and PGAM2-WT or PGAM2-K100R, and found that PGAM2-WT interacted with SIRT2 more intensively than PGAM2-K100R (Fig. 3F). Then we transfected plasmids expressing PGAM2 and ubiquitin into HEK293T cells along with SITR2 or control. Results showed that the ubiquitination level of PGAM2 was markedly enhanced by SIRT2 overexpression (Fig. 3G). These results demonstrate that PGAM2 was deacetylated by SIRT2, which primarily functions at the K100 site.

Next, we determined the effects of SIRT2 on PGAM2 expression and HCC progression. Results showed that overexpression of SIRT2 decreased PGAM2 expression (Fig. 3H), while inhibition of SIRT2 enhanced the protein level of PGAM2 (Fig. 3I, Supplementary Fig. S1A). Accordingly, we found that overexpression of SIRT2 rescued the inhibitory effects of PGAM2 on cell growth and colony formation, while it attenuated apoptosis of HCC cells induced by PGAM2 overexpression (Fig. 3J–L). Moreover, knockdown of SIRT2 by siRNA attenuated the promoting effects of PGAM2 knockdown on cell growth and colony formation (Supplementary Fig. S1B–D). Collectively, these results demonstrate that SIRT2-mediated deacetylation modification downregulates PGAM2 to promote HCC progression.

PGAM2 suppresses aerobic glycolysis in HCC cells

Given that PGAM2 is an important glycolytic enzyme (Fig. 4A), we explored the biochemical significance of PGAM2 in aerobic glycolysis in HCC cells. Results showed that PGAM2 overexpressing cells exhibited decreased glucose uptake and extracellular lactate level compared to controls, whereas PGAM2 knockdown cells showed an increase in both parameters (Fig. 4B–E). Similarly, both deacetylation of PGAM2 at K100 and overexpression of SIRT2 promoted glucose consumption and lactate production, while silencing of SIRT2 weakened the effects of PGAM2 knockdown on aerobic glycolysis (Fig. 4F, G, Supplementary Fig. S1E). Additionally, we evaluated the expression levels of crucial glycolytic enzymes, and results showed that Hexokinase-2 (HK2), Glyceraldehyde-3-phosphate dehydrogenase (GAPDH), Phosphoglycerate mutase 1 (PGAM1), Pyruvate kinase 2 (PKM2), and lactate dehydrogenase A (LDHA) were significantly up-regulated in both PGAM2 knockdown and PGAM2-K100R expressing cells. Conversely, these enzymes were down-regulated in PGAM2 overexpressing cells (Fig. 4H, I). These results suggest that PGAM2 plays a negative role in aerobic glycolysis in HCC cells.

Knockdown of PGAM2 promotes aerobic glycolysis by activating the STAT3/LDHA axis

LDHA plays a vital role in glycolysis, which converts pyruvate to lactate. Next, we explored whether PGAM2 knockdown promoted HCC progression via LDHA-mediated aerobic glycolysis. We found that

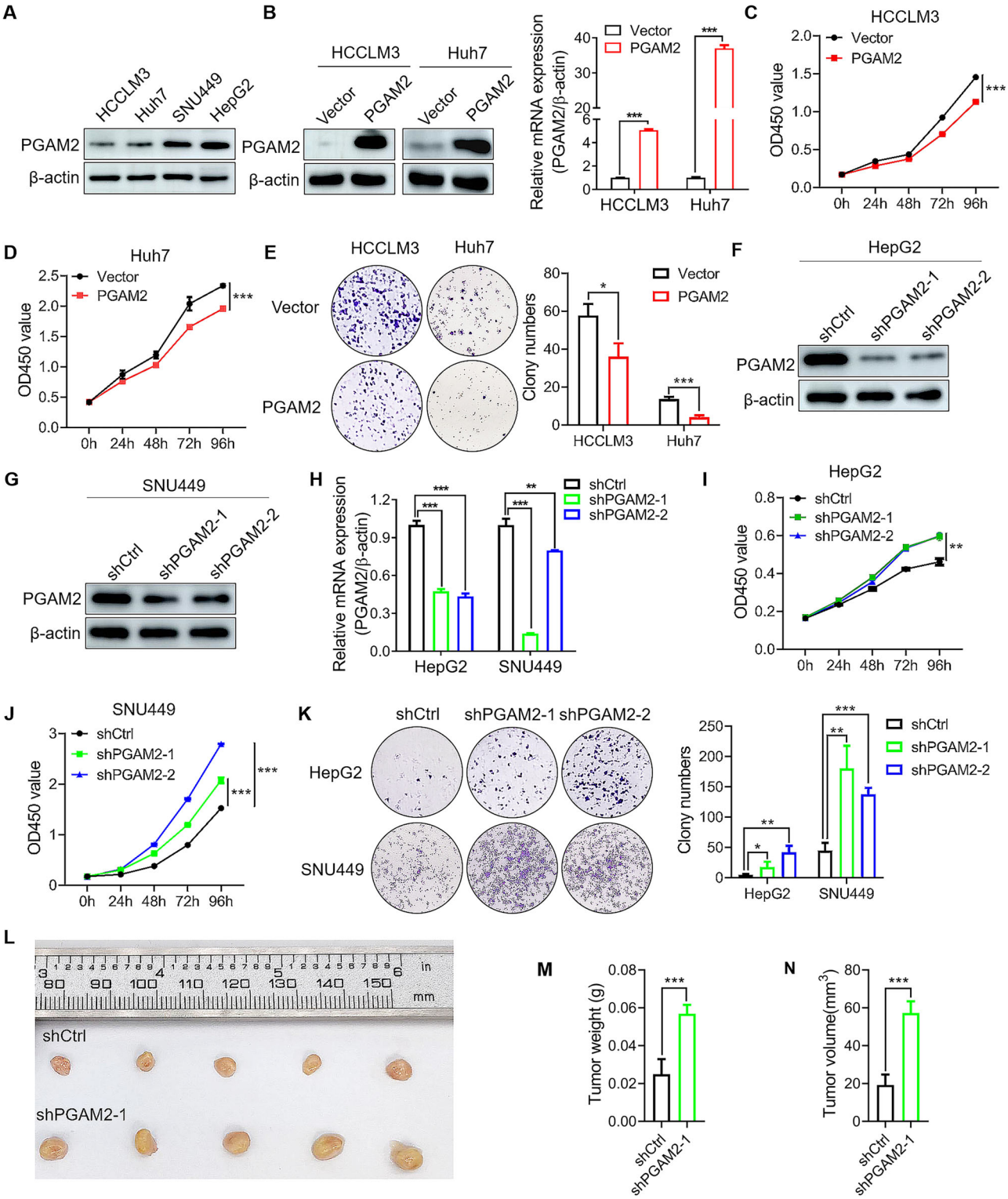

Fig. 1 | Knockdown of PGAM2 promotes proliferation and tumor growth of HCC cells both in vitro and in vivo. A PGAM2 levels in HCC cell lines were detected by western blot. **B** Detection of PGAM2 protein and mRNA levels by western blot and RT-qPCR in PGAM2 overexpression cells and controls. **C**–**E** Cell growth rates and colony formation abilities detection of PGAM2 overexpressing cells and controls. **F**–**H** Detection of PGAM2 protein and mRNA levels by western blot and RT-qPCR in PGAM2 knockdown cells and controls. **I**–**K** Cell growth rates and colony formation abilities detection of PGAM2 knockdown cells and controls. **L**–**N** Representative image, volume and weight of xenografts with PGAM2 knockdown cells or controls ($n = 5$). $^{*}p < 0.05$, $^{**}p < 0.01$, $^{***}p < 0.001$.

overexpression of LDHA reversed the inhibitory effect of PGAM2 on glycolysis, while LDHA knockdown lead to a reduction in glucose uptake and lactate production in PGAM2 knockdown cells (Supplementary Fig. S2A–C, Fig. 5A). Besides, enzymatic activity inhibition of LDHA with sodium oxamate diminished the promoting effect of PGAM2 inhibition on glucose uptake and lactate production (Supplementary Fig. S2D). Moreover, the inhibitory effects of PGAM2 on cell viability and colony formation were rescued by LDHA

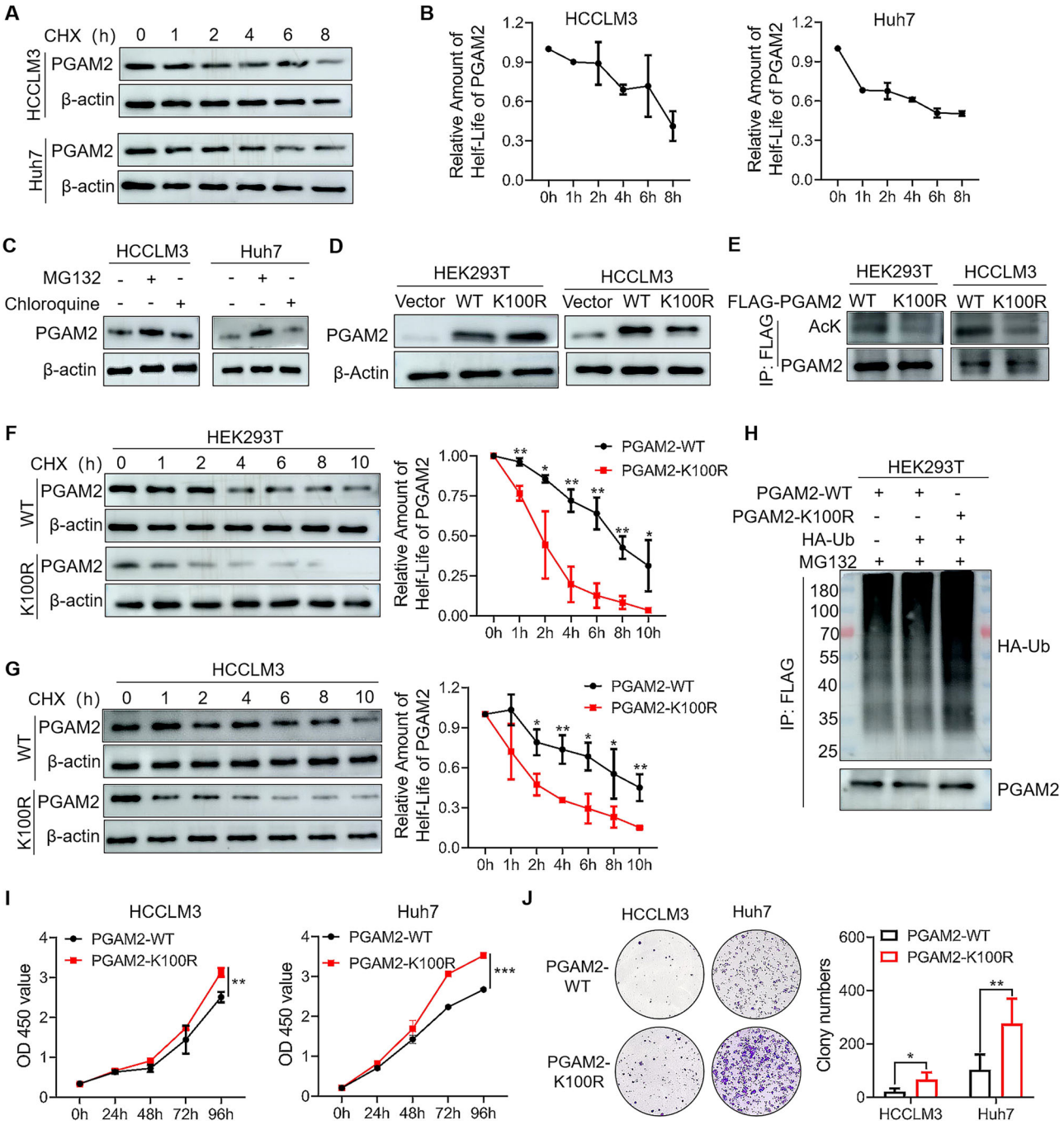

Fig. 2 | Deacetylation of PGAM2 at K100 promotes its ubiquitination and degradation. A Half-life of PGAM2 was analyzed by western blot in HCC cell lines treated with 200 μg/mL cycloheximide (CHX) for indicated hours. **B** The curves were completed based on the gray value quantification of the bands in (**A**). **C** PGAM2 was measured by western blot in HCC cell lines treated with 25 μM proteasome inhibitor MG132 or 50 μM lysosome inhibitor Chloroquine for 16 h. **D** Construction and western blot analysis of HEK293T and HCCLM3 cell lines expressing PGAM2 wild type (PGAM2-WT) or deacetylation-mimic (PGAM2-K100R) proteins. **E** Acetylation levels of PGAM2-WT and PGAM2-K100R were detected by Co-IP. **F, G** Half-life of PGAM2-WT and PGAM2-K100R were detected by western blot in HEK293T and HCCLM3 cell lines treated with 200 μg/mL CHX. **H** Exogenous PGAM2-WT, PGAM2-K100R, and ubiquitin-expressing plasmids were transfected into HEK293T cells, then ubiquitination levels of PGAM2-WT and PGAM2-K100R were measured by Co-IP after being treated with 25 μM MG132 for 16 h. **I, J** Cell growth rates and colony formation abilities detection of PGAM2-WT and PGAM2-K100R expressing HCC cell lines. $^{*}p < 0.05$, $^{**}p < 0.01$, $^{***}p < 0.001$.

overexpression, while inhibition of LDHA expression or enzymatic activity attenuated the promoting effect of PGAM2 knockdown on cell proliferation and colony formation (Fig. 5B, C, Supplementary Fig. S2E, F). These data suggest that PGAM2 suppresses aerobic glycolysis and proliferation of HCC cells through inhibiting LDHA expression.

Then we explored the mechanism underlying PGAM2-mediated LDHA expression in HCC cells. Based on the JASPAR (http://jaspar.genereg.net/) database, we identified that STAT3 mainly bind to the proximal region (2000bp upstream) of *LDHA* promoter, which was validated by ChIP-qPCR and dual-luciferase reporter assays (Fig. 5D–F). Besides, the correlation analysis from the Gene Expression Profiling Interactive Analysis database indicated that the expression levels of *STAT3* and *LDHA* in HCC patients had a high co-expression correlation coefficient of 0.54 (Supplementary Fig. S2G). We also found that the level of p-STAT3 decreased in PGAM2

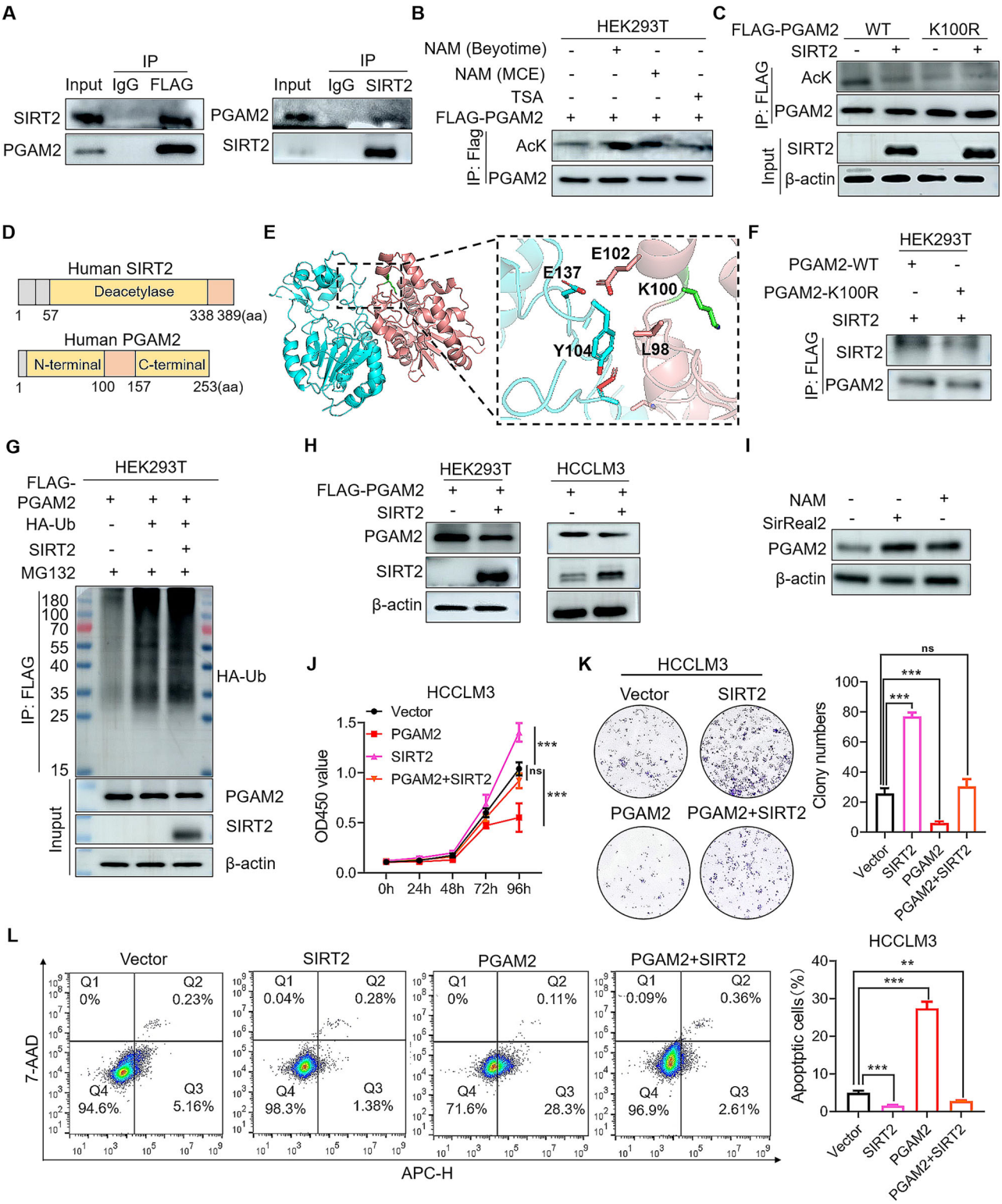

overexpressing cells while PGAM2 knockdown enhanced the expression level and nuclear localization of p-STAT3 (Fig. 5G, H, Supplementary Fig. S3A). Additionally, inhibition of STAT3 activation with stattic not only decreased the mRNA and protein levels of LDHA, but also weakened the proliferation and colony formation abilities of PGAM2 knockdown cells. (Fig. 5I, J, Supplementary Fig. S3B–D). Taken together, these findings prove that knockdown of PGAM2 promotes LDHA expression through STAT3 activation.

Knockdown of PGAM2 enhances the sensitivity of HCC cells to sorafenib

Sorafenib serves as the first-line treatment for advanced HCC. To investigate the impact of PGAM2 on the anti-tumor effect of sorafenib on HCC cells, we treated PGAM2 knockdown cell lines and controls with sorafenib, and found that the IC50 values of sorafenib in PGAM2 knockdown cells were much lower than those in controls (Fig. 6A–C). Besides, PGAM2 knockdown cells exhibited lower cell proliferation rates compared to controls

Fig. 3 | SIRT2 deacetylates PGAM2 to promote HCC progression. A Plasmids expressing Flag-PGAM2 and SIRT2 were transfected into HEK293T cells and lysates were co-immunoprecipitated with FLAG or SIRT2 antibodies and then immunoblotted with indicated antibodies. **B** Acetylation level of PGAM2 was detected by Co-IP in HEK293T cell line treated with 40 mM SIRTs family inhibitor Nicotinamide (NAM) or 20 μM HDAC I/II family inhibitor Trichostatin A (TSA) for 12 h. **C** Plasmids expressing PGAM2-WT and PGAM2-K100R were transfected into HEK293T cells with or without SIRT2-expressing plasmid, then acetylation levels of PGAM2-WT and PGAM2-K100R were detected by Co-IP. **D** Schematic of the domain structure of PGAM2 and SIRT2. **E** Interaction between SIRT2 and PGAM2 was analyzed by pymol, PGAM2 (red), SIRT2 (blue). **F** Plasmid expressing PGAM2-WT or PGAM2-K100R were transfected into HEK293T cells along with SIRT2-expressing plasmid, then the binding abilities between SIRT2 and PGAM2-WT or PGAM2-K100R were detected by Co-IP. **G** Exogenous Flag-PGAM2 and ubiquitin-expressing plasmids were transfected into HEK293T cells with or without SIRT2-expressing plasmid, then ubiquitination levels of PGAM2 was measured by Co-IP after treatment with 25 μM MG132 for 16 h. **H** PGAM2 was overexpressed in HEK293T and HCCLM3 cell lines along with SIRT2 or not, and cell lysates were used to examine the level of PGAM2 by western blot. **I** PGAM2 was measured by western blot in HCCLM3 cell line treated with 40 mM NAM or 20 μM SIRT2 inhibitor SirReal2 for 12 h. **J**, **K** Cell growth rates and colony formation abilities detection of HCCLM3 cell lines overexpressing Vector, PGAM2, SIRT2 alone or in combination. **L** Detection of cell apoptosis rates of HCCLM3 cell lines over-expressing Vector, PGAM2, SIRT2 alone or in combination. $^{**}p < 0.01$, $^{***}p < 0.001$, ns no significance.

treated with sorafenib (Fig. 6D–F), which suggests that knockdown of PGAM2 enhances the sensitivity of HCC cells to sorafenib. Since we have proved that PGAM2 was down-regulated by SIRT2, then the function of SIRT2 in tumor growth and sorafenib sensitivity of HCC was detected. Results showed that inhibition of SIRT2 with AGK2 had similar effect as sorafenib in reducing tumor burden (Fig. 6G–I). However, we found that SIRT2 was increased in sorafenib resistant HCC cells (Fig. 6J, K), and HCC patients with higher SIRT2 levels showed shorter overall survival and progression free survival after treatment with sorafenib (Fig. 6L, M), which suggests that SIRT2 possibly contributes to sorafenib resistance of HCC cells. Accordingly, we found that combination of AGK2 and sorafenib significantly decreased the cell viability compared with sorafenib treatment alone (Fig. 6N, O), which indicates that inhibition of SIRT2 reduces sorafenib resistance of HCC cells.

SIRT2 negatively correlates with PGAM2 in HCC tissues

To explore the clinical significance of PGAM2 in HCC, we measured PGAM2 expression in twenty-one pairs of tumor and adjacent normal liver tissues from HCC patients. Results showed that the protein level of PGAM2 was down-regulated in tumor tissues (Fig. 7A, Supplementary Fig. S4A). Since we have demonstrated that the expression level of SIRT2 was up-regulated in HCC tissues[15], here we analyzed the correlation between SIRT2 and PGAM2. It showed that SIRT2 was negatively correlated with PGAM2 in HCC tissues (Fig. 7B). Accordingly, the protein level of PGAM2 was down-regulated while that of SIRT2 was up-regulated in HCC tissues based on the UALCAN/CPTAC database (Fig. 7C). Moreover, the expression levels of both *SIRT2* and *LDHA* positively correlated with the clinical stage of HCC patients (Fig. 7D). We also evaluated the prognostic value of *SIRT2* and *LDHA* in HCC patients based on the TCGA database. Results showed that high expression levels of both *SIRT2* and *LDHA* were correlated with poor overall survival and recurrence free survival in HCC patients (Fig. 7E, F). Overall, these clinical data provide SIRT2 and LDHA as potential prognostic markers and therapeutic targets for HCC.

Discussion

Mammalian PGAM consists of two isoforms, PGAM1 and PGAM2, which share sequence homology and conserved enzymatic activity[20]. While PGAM1 has been well-characterized as an oncogenic driver that facilitates tumorigenesis and progression by enhancing glycolysis[21], the role of PGAM2 in HCC remains poorly understood. In this study, we identified PGAM2 as a tumor suppressor that was significantly down-regulated in HCC tissues. Previous studies have shown that PGAM2 undergoes MDM2-mediated ubiquitination modification, which possibly occurs on lysine sites between K100 and K157[18]. Here we specifically demonstrated that K100 served as the predominant deacetylation site in PGAM2 and played a critical role in regulating its ubiquitination and degradation. These findings not only establish a regulatory link between deacetylation and protein stability, but also expand our understanding of PGAM2 down-regulation mechanisms beyond genomic or transcriptional regulation to include post-translational control. Furthermore, we found the protein level of PGAM2 decreased in most kinds of cancers while its transcription level was mostly up-regulated or unchanged in tumor tissues (Supplementary Fig. S4B, C). This discrepancy strongly suggests that post-translational regulation represents the primary mechanism underlying PGAM2 down-regulation in cancers.

In this study, we identified SIRT2 as the deacetylase responsible for deacetylation of PGAM2 at K100 site and down-regulated PGAM2 expression in HCC cells. Intriguingly, we observed that knockdown of PGAM2 enhanced sorafenib sensitivity in these cells, suggesting that SIRT2-mediated PGAM2 down-regulation might increase drug responsiveness. This finding appears contradictory to established evidence demonstrating SIRT2 overexpression in sorafenib resistant HCC cells, where its inhibition actually restores therapeutic sensitivity[22]. SIRT2 has been shown to promote sorafenib resistance through multiple mechanisms, such as drug-resistance mediators, metabolic reprogramming, EMT, and so on[23–26]. Notably, our results revealed significant down-regulation of PGAM2 in sorafenib resistant HCC cells compared to the control (Supplementary Fig. S4D). These collective findings suggest a dual regulatory paradigm: while SIRT2-mediated PGAM2 suppression may transiently enhance sorafenib sensitivity in treatment-naive cells, the development of acquired resistance appears to involve alternative SIRT2-driven mechanisms that ultimately dominate the cellular response. This mechanistic shift likely explains the clinically observed correlation between SIRT2 overexpression and therapeutic resistance. More importantly, it suggests that combination of SIRT2 inhibitors with sorafenib may represent a novel strategy to improve clinical outcomes in sorafenib-resistant HCC patients.

Metabolic enzymes usually exert dual roles through both enzymatic activity-dependent and -independent mechanisms. Here we found that deacetylation or knockdown of PGAM2 enhanced aerobic glycolysis in HCC cells. Intriguingly, studies have shown that nuclear-localized PGAM2 contributes to nucleolar integrity maintenance, transcriptional regulation, and pre-ribosomal assembly[20], while cytoplasmic PGAM2 is implicated in promoting oncogenesis through enzymatic activity-independent mechanisms[7,8]. These findings collectively suggest that PGAM2 may drive cancer progression via non-metabolic functions. In this study, we identified LDHA, a critical mediator of aerobic glycolysis overexpressed in malignancies[27,28], as the downstream effector of PGAM2. We found that PGAM2 knockdown upregulated LDHA expression via STAT3 activation, while the mechanism for STAT3 activation in PGAM2 knockdown cells was not expounded, which needs to be deciphered in future studies and may provide more evidence for PGAM2 participating in cancer progression in an enzymatic activity-independent manner.

STAT3 is an oncogenic transcription factor dysregulated in approximately 70% of cancers[29–31]. It has been discovered that STAT3 functions as an upstream transcription factor of LDHA in bladder cancer and ovarian cancer, thereby augmenting LDHA transcription to facilitate cancer glycolysis and progression[32,33]. Crucially, inhibition of either p-STAT3 or LDHA abrogated the pro-tumorigenic effects induced by PGAM2 knockdown. These findings not only delineate the STAT3/LDHA axis as a key mediator of PGAM2-dependent HCC progression, but also highlight them as promising therapeutic targets.

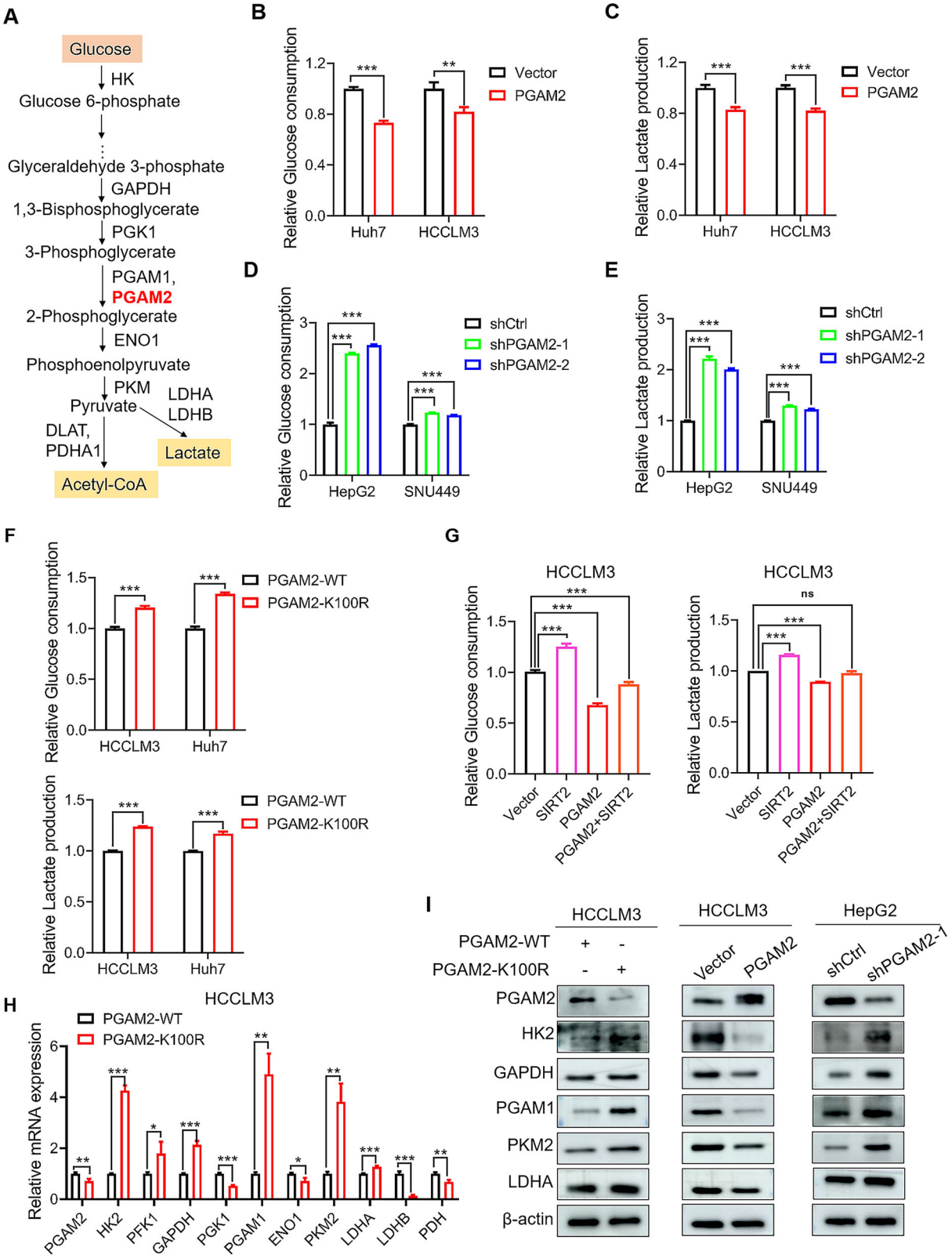

Fig. 4 | PGAM2 suppresses aerobic glycolysis and key enzymes expression in HCC cells. A Schematic representation of aerobic glycolysis and key enzymes involved. **B**–**G** Detection of glucose consumption and lactate production in PGAM2 overexpressing cell lines and controls; PGAM2 knockdown cell lines and controls; PGAM2-WT and PGAM2-K100R expressing cell lines; and cell lines overexpressing Vector, PGAM2, SIRT2 alone or in combination. **H** mRNA levels of key glycolytic enzymes were detected by RT-qPCR in HCCLM3 cell lines expressing PGAM2-WT and PGAM2-K100R. **I** Protein levels of key enzymes were detected by western blot in PGAM2-WT and PGAM2-K100R expressing cell lines; PGAM2 overexpressing cell lines and controls; PGAM2 knockdown cell lines and controls. $^{*}p < 0.05$, $^{**}p < 0.01$, $^{***}p < 0.001$, ns no significance.

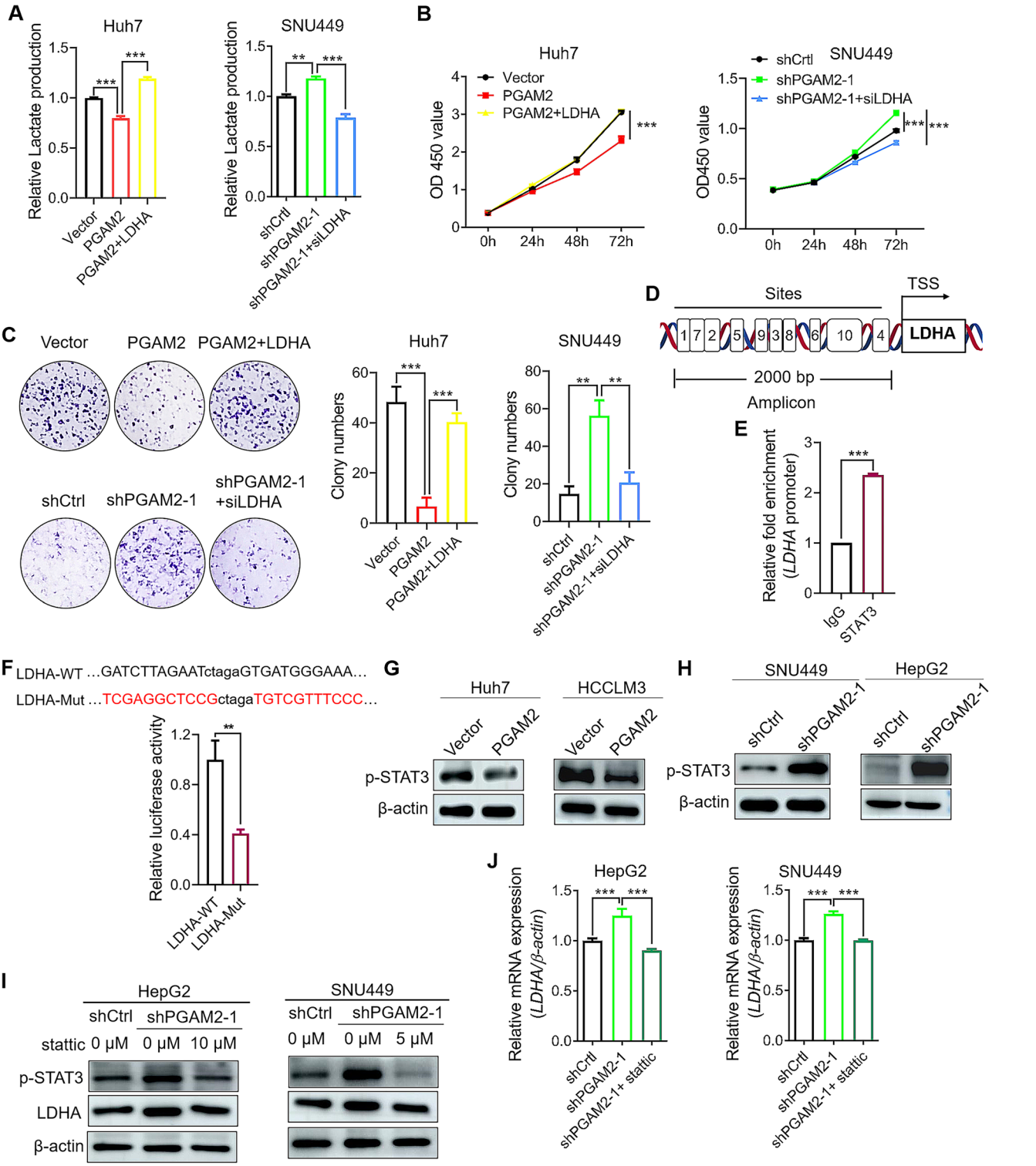

Fig. 5 | Knockdown of PGAM2 enhances glycolysis by promoting STAT3-mediated LDHA expression in HCC cells. A–C Detection of lactate production, growth rate, and colony formation ability of HCC cell lines with PGAM2, LDHA overexpression or knockdown. **D** Schematic model of STAT3 binding sites to *LDHA* promoter. **E** ChIP-qPCR analysis of *LDHA* promoter region binding to STAT3 in SNU449 cell line. IgG is included as the control for IP. **F** Dual-luciferase reporter assay to identify the binding of STAT3 to *LDHA* promoter. **G**, **H** Detection of p-STAT3 in PGAM2 overexpressing and knockdown HCC cell lines by western blot. **I**, **J** Protein and mRNA levels of LDHA were detected by western blot and RT-qPCR in controls and PGAM2 knockdown cells treated with or without STAT3 inhibitor stattic. $^{**}p < 0.01$, $^{***}p < 0.001$.

In conclusion, our study elucidates that SIRT2-mediated deacetylation of PGAM2 at K100 facilitates its ubiquitination and degradation, and then promotes HCC progression by amplifying aerobic glycolysis through a non-enzymatic mechanism involving STAT3-mediated transcription activation of LDHA(Fig. 7G). These findings reveal a novel mechanism wherein SIRT2-dependent post-translational modification of PGAM2 reprograms cellular metabolism to promote HCC progression, and provide valuable biomarkers and therapeutic targets for HCC.

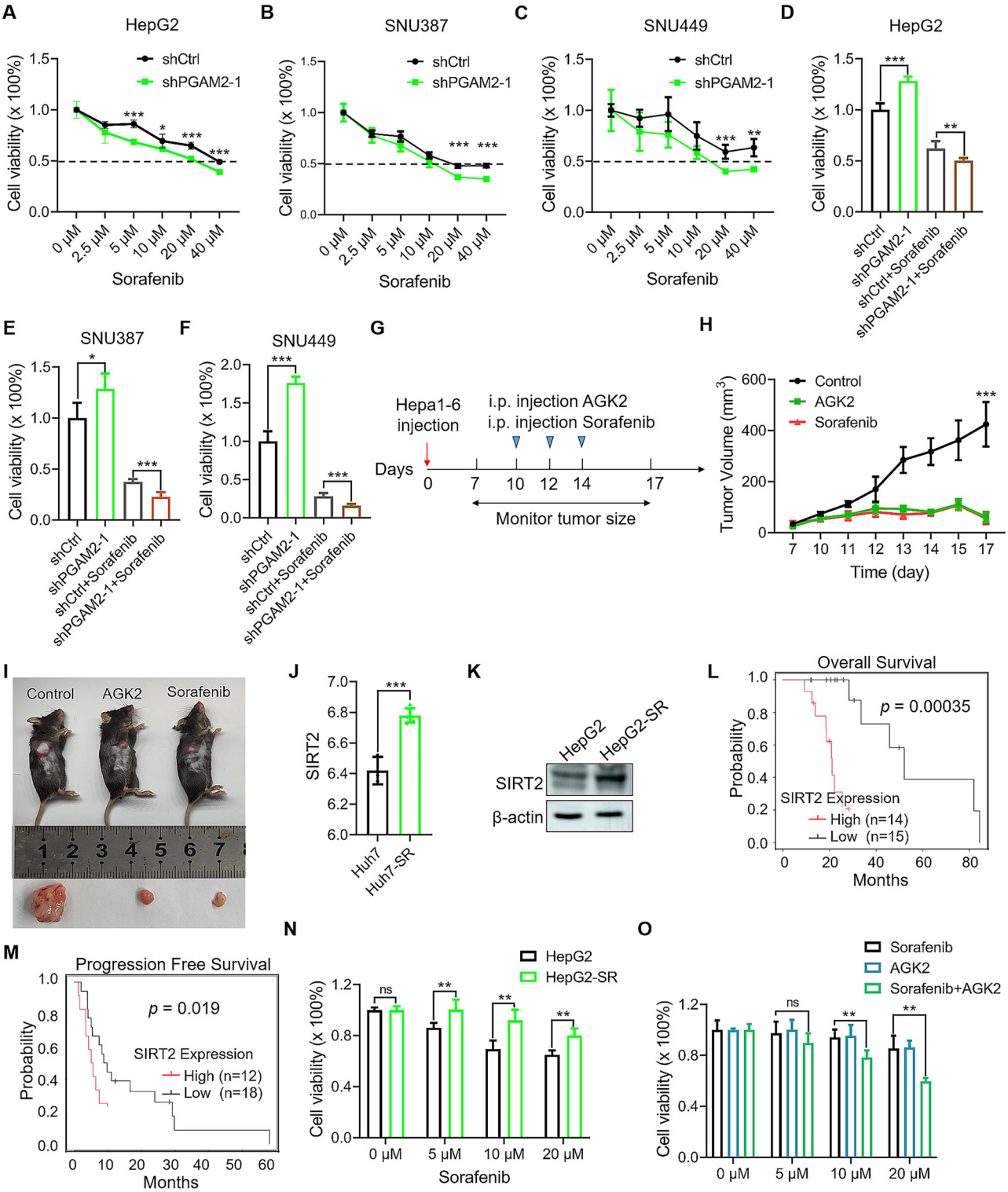

Fig. 6 | Knockdown of PGAM2 enhances sorafenib sensitivity of HCC cells. **A**–**C** Cell viability of controls and PGAM2 knockdown HCC cell lines treated with sorafenib for 48 h was detected by cck8 assay. **D**–**F** Cell viability of controls and PGAM2 knockdown HCC cell lines treated with or without sorafenib (40 μM for HepG2 and SNU449, 10 μM for SNU387) for 48 h was detected by cck8 assay. **G** Diagram illustrates treatment groups and timetable of injection of sorafenib or AGK2. **H** Tumor volume was measured with indicated treatment ($n = 4$). **I** Imaging of tumors in vivo and derived from mice ($n = 4$). **J** Expression level of *SIRT2* in normal and sorafenib resistant Huh7 cell lines based on TCGA database. **K** Detection of SIRT2 in normal and sorafenib resistant HepG2 cell lines by western blot. **L**, **M** Kaplan–Meier curve of overall survival and progression free survival of HCC patients after sorafenib treatment according to *SIRT2* expression in tumors based on TCGA database. **N** Cell viability detection of normal and sorafenib resistant HepG2 cell lines treated with sorafenib for 48 h by cck8. **O** Cell viability detection of sorafenib resistant HepG2 cell line treated with sorafenib and AGK2 alone or in combination for 48 h. SR sorafenib resistant, $^{*}p < 0.05$, $^{**}p < 0.01$, $^{***}p < 0.001$, ns no significance.

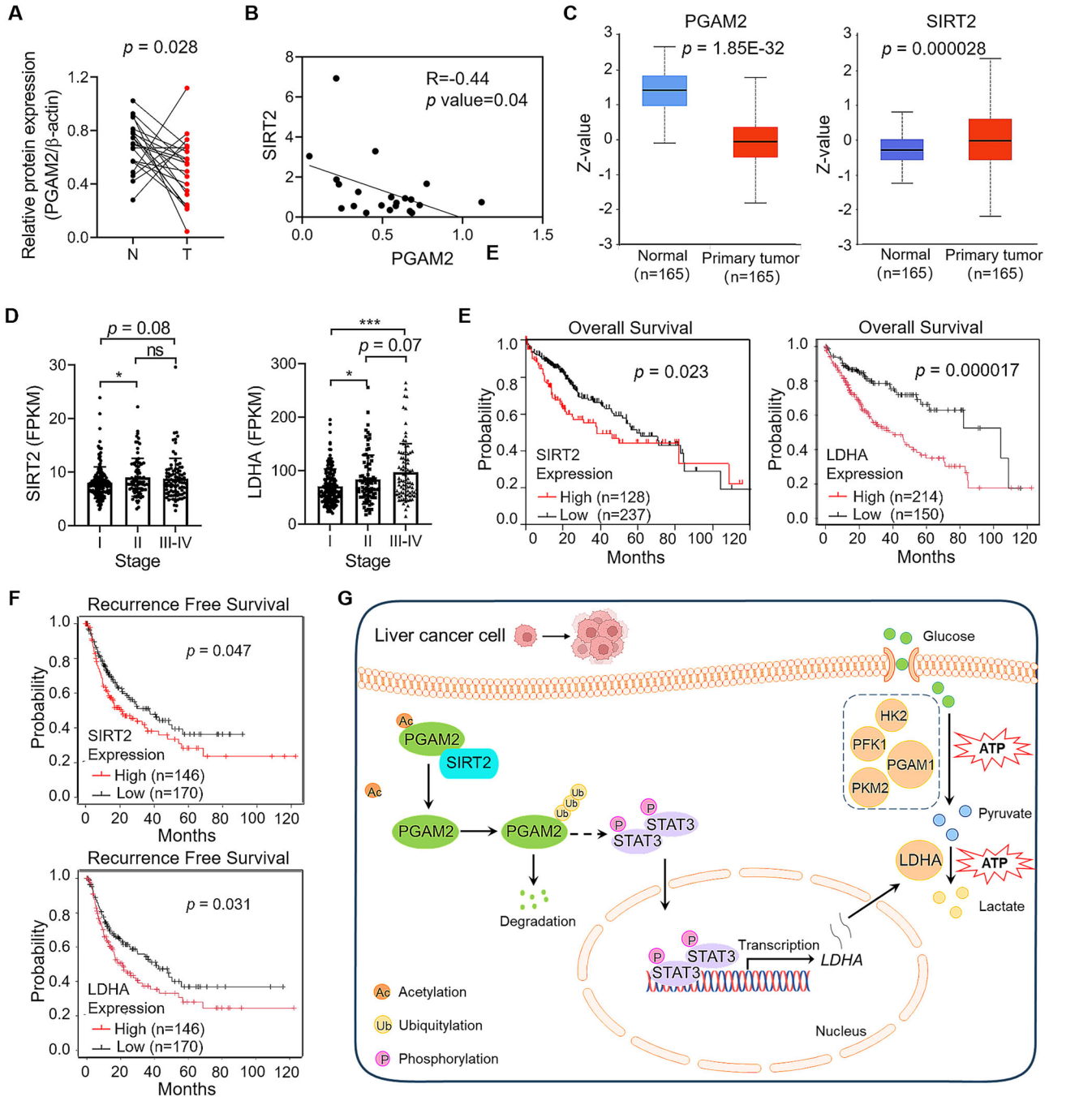

Fig. 7 | PGAM2 negatively correlates with PGAM2 in HCC tissues. A Statistical analysis of relative PGAM2 expression in paired samples from HCC patients ($n = 21$). **B** Correlation analysis of PGAM2 and SIRT2 in HCC tissues ($n = 21$). **C** Protein levels of PGAM2 and SIRT2 in HCC tissues compared with adjacent normal liver tissues based on CPTAC database. **D** *SIRT2* and *LDHA* levels in HCC tissues from different clinical stages. **E, F** Kaplan–Meier curves of overall survival and recurrence free survival according to *SIRT2* or *LDHA* levels in HCC tumors based on TCGA database. **G** Schematic model of the role of SIRT2-mediated deacetylation of PGAM2 in promoting HCC progression through activating STAT3/LDHA axis. N normal liver tissue, T tumor tissue, $^{*}p < 0.05$, $^{***}p < 0.001$, ns no significance.

Methods

Tissue samples

Paired tumor and adjacent normal liver tissues ($n = 21$) were obtained from HCC patients in the First Affiliated Hospital of Zhengzhou University (Supplementary Table S1). Tissue samples were surgically removed when patients were identified with HCC for the first time, and the patients did not receive any treatment before surgery. This study was approved by the Research Ethics Committee of Zhengzhou University (No. YLL-019), and was conducted Declaration of Helsinki. All of the individuals participating in this study have provided written informed consent.

Cell lines and reagents

HEK293T cell line and human HCC cell lines including HCCLM3, Huh7, SNU449, HepG2, and SNU387 were cultured in DMEM or RPMI-1640 (HyClone, Utah, USA) medium supplemented with 10% fetal bovine serum (FBS) (Gibco, New York, USA) at 37° °C and 5% CO_2. Mouse liver cancer cell line Hepa1-6 was cultured in DMEM medium with 10% FBS. All the cell lines were performed with STR authentication. Reagents: Cycloheximide (MCE, HY-12320, New Jersey, USA); MG132 (MCE, HY-13259); Chloroquine (MCE, HY-17589A); AGK2 (Beyotime, SC0285, Shanghai, China); SirReal2 (Beyotime, SC0290); Nicotinamide (MCE, HY-B0150; Beyotime,

S1761); Trichostatin A (Beyotime, S1893); Puromycin (Solarbio, P8230, Beijing, China); G418 (BBI Life Sciences, A600958, Shanghai, China); Sodium oxamate (Merck KGaA, 02751, Darmstadt, Germany); Stattic (MCE, HY-13818); Sorafenib (Aladdin, s125098, Shanghai, China).

Lentivirus construction and transduction

Lentivirus expressing PGAM2-WT, PGAM2-K100R, LDHA, and SIRT2 were constructed with HEK293T cells. Briefly, vectors and lipo2000 (Invitrogen, 11668-019, Shanghai, China) were added to the culture medium when cell density reached 80% confluence. The culture medium containing lentiviral particles were collected 48 h later, filtered with 0.22 μm filter, and stored at −80 °C. Lentivirus expressing short hairpin RNAs (shRNAs) targeting PGAM2 were purchased from GENE (Shanghai, China). Stable cell lines were selected using puromycin (2 μg/mL) or G418 (100 μg/mL).

Construction of PGAM2-WT and PGAM2-K100R expressing cell lines

First, cell lines were transfected with shRNA virus to knockdown endogenous PGAM2, then PGAM2-WT and PGAM2-K100R overexpressing virus were transfected into PGAM2 knockdown cell lines. The nucleotide sequence targeted by shRNA in exogenous PGAM2-WT and PGAM2-K100R coding sequences was performed with synonymous mutation.

Transient transfection

Small interfering RNAs (siRNAs) were synthesized by RiboBio, (Guangzhou, China). The transfection complex was prepared in the following manner: 1.25 μL of 20 μM siRNA storage solution was added to 30 μL of 1× riboFEC^{TM} CP Buffer and mix gently. Then 3 μL of riboFECT^{TM} CP Reagent was added to this mixture and incubated for 15 min at room temperature. The transfection complex was added to the cells and mixed gently. Cells were incubated in a CO_2 incubator at 37 °C for 24-96 h. The siRNA sequences were listed in Supplementary Table S2.

Western blot

Cells were lysed in RIPA buffer (Servicebio, G2002, Wuhan, China) supplemented with phenylmethylsulfonyl fluoride (PMSF) (a serine protease inhibitor, Servicebio, G2008) and Deacetylase Inhibitor Cocktail (MCE, HY-K0030) for 30 min. The supernatant was collected and protein concentrations were determined using a BCA kit (BBI Life Sciences, C503021). After the proteins were quantified and denatured, samples were separated by SDS-PAGE electrophoresis and then transferred onto PVDF membrane (Merck Millipore, IPVH00010). The membranes were blocked with 5% nonfat milk solution for 2 h at room temperature, incubated with primary antibody overnight at 4 °C and then reacted with HRP-conjugated secondary antibody for 2 h at room temperature. Protein level was quantified using Image J software, and normalized by β-actin. Information of antibodies were listed in Supplementary Table S3.

Co-immunoprecipitation (Co-IP)

Antibodies were incubated with 20 μL of protein A/G magnetic beads (Bimake, B23202, Texas, USA) with constant rotation for 30 min, followed by incubation with Cell lysates at room temperature for 1 h. The immunoprecipitants were washed three times, and then eluted with SDS-loading buffer. Proteins were incubated at 95 °C for 10 min before detection.

Quantitative reverse transcription PCR (RT-qPCR)

Total RNA was extracted using TRIzol reagent (Vazyme Biotech, R401-01, Nanjing, China) following the manufacturer's instructions and cDNA was synthesized using the PrimeScript RT Reagent Kit (TaKaRa Clontech, RR036, Dalian, China). Then qPCR was performed by using the ChamQ^{TM} Universal SYBR$^{®}$ qPCR Master Mix (Vazyme Biotech, Q711) and QuantStudio 5 Real-Time PCR System (Thermo Scientific, Massachusetts, USA). The mRNA expression levels were normalized by β-actin and quantified by comparative CT ($2^{-\Delta\Delta Cq}$) as previously described[3,4]. Sequences for RT-qPCR analysis were listed in Supplementary Table S2.

CCK-8 assay

Cells in the logarithmic growth phase were seeded in a 96-well plate (3000 cells/100 μL/well). At 0, 24, 48, 72, and 96 h, 10 μL of CCK-8 reagent (Vazyme, A311) was added to the culture medium and incubated for 2 h at 37 °C in the dark. Absorbance (A) was measured at 450 nm using a microplate reader (Thermo, USA).

Colony formation assay

A total of 2000 cells were added to a well of six-well plate and incubated in a CO_2 incubator at 37 °C for 10-14 days. The colonies formed were fixed with 4% paraformaldehyde (Leagene, DF0141, Beijing, China) for 30 min and stained with 0.5% crystal violet. The number of colonies was counted and analyzed.

Cell apoptosis assay

This assay was performed using Annexin V-Allophycocyanin/7-Amino Actinomycin D Apoptosis Detection Kit (KeyGEN, KGA1106, Nanjing, China). Briefly, cells were digested using EDTA-free trypsin, and washed with PBS for twice. Then 5 μL Annexin V-APC and 7-AAD were added after cells were suspend by 500 μL binding buffer. Cells were incubated in the dark for 15 min at room temperature, and then analyzed using ACEA NovoCyte3130 within 1 h.

In vivo experiments

The in vivo study was approved by the Animal Ethics Committee of Zhengzhou University (No. 2023-YYY-088). The mice were housed under specific pathogen-free (SPF) condition with free access to food and water, and they were sacrificed by cervical dislocation at the end of the experiment.

For xenograft mice model, three-week old female nude mice were purchased from the Beijing Charles River Laboratory Technology Co. The mice were randomly divided into two groups, and approximately 8×10^6 cells were suspended in 100 μL PBS and injected subcutaneously into nude mice after they were housed for one week. Tumor growth was regularly measured. 21 days later, the mice were sacrificed.

For AGK2 and sorafenib treatment in vivo, five-week old C57BL/6 male mice were purchased from HFKBIO. The model was established by subcutaneously injecting 1×10^6 Hepa1-6 cells into the right armpit of mice. Mice were randomly divided on day 7, and treated i.p. with 15 mg/kg AGK2 or 60 mg/kg sorafenib for three times a week. Mice were sacrificed on day 17.

The tumor size did not exceed the permitted maximal volume of 1000 mm^3. Tumors in the mice were isolated, weighed, and photographed. Tumor volumes were calculated using the following formula: tumor volume = $(width^2 \times length)/2$.

Glucose and lactate content measurement

Cells were cultured in 24-well plates seeded at 2×10^5 cells per well for 48 h. Then culture medium was then collected. Glucose and lactate contents were measured with absorption at 450 nm by using Glucose Assay Kit (Bestbio, BB-47305, Shanghai, China) and Lactate Assay Kit (Jiancheng Bioengineering, A019-2-2, Nanjing, China). Glucose and lactate contents were quantified according to the standards.

Chromatin immunoprecipitation quantitative polymerase chain reaction (ChIP-qPCR)

Cells (8×10^6) were prepared for the ChIP-qPCR assay using a ChIP Assay Kit (Beyotime, P2078). Briefly, the nuclei were extracted in SDS lysis buffer containing 1 mM PMSF and subsequently subjected to ultrasound treatment (70 W, 120 s). 60 μL Protein A + G Agarose/Salmon Sperm DNA was added to the sample, which was placed on a rotating mixer and slowly rotated at 4 °C for 30 min. Then samples were centrifuged at 1000 g at 4 °C for 1 min, and the supernatant was transferred to a new tube and 4 μl anti-STAT3 antibody was added. At the same time, IgG antibody was added as a negative control and incubated overnight at 4 °C. Then 80 μL Protein A + G Agarose/Salmon Sperm DNA was added to the tube, and rotated at 4 °C for 60 min. After washing for thrice, the DNA was recovered with a DNA recovery kit and analyzed using qPCR.

Dual-luciferase reporter assay

The binding sites of STAT3 on LDHA promoter region were predicted through JASPAR database. The wild type and mutant sequences of the binding sites were synthesized and constructed into the pGL3-basic plasmid, and then co-transfected with pcDNA3.1-STAT3 expressing plasmid and Renilla luciferase reporter plasmid into HEK293T cells for 48 h. The luciferase activities were measured with the Dual Luciferase Reporter Gene Assay (Yeasen Biotechnology, 11402ES60, Shanghai, China).

Statistical analysis

Data were analyzed using GraphPad Prism 8.0 software. The experiments were repeated at least three times independently, and data were presented as mean ± standard deviation (SD). All analyses were two-sided, and $p < 0.05$ was considered to indicate a statistically significant difference.

Data availability

No datasets were generated or analyzed during the current study.

Received: 7 November 2024; Accepted: 30 April 2025;
Published online: 16 May 2025

References

1. Kim, E. & Viatour, P. Hepatocellular carcinoma: old friends and new tricks. *Exp. Mol. Med.* **52**, 1898–1907 (2020).
2. Sung, H. et al. Global Cancer Statistics 2020: GLOBOCAN Estimates of Incidence and Mortality Worldwide for 36 Cancers in 185 Countries. *CA Cancer J. Clin.* **71**, 209–249 (2021).
3. Akinyemiju, T. et al. The Burden of Primary Liver Cancer and Underlying Etiologies From 1990 to 2015 at the Global, Regional, and National Level: Results From the Global Burden of Disease Study 2015. *JAMA Oncol.* **3**, 1683–1691 (2017).
4. Siegel, R. L., Miller, K. D., Fuchs, H. E. & Jemal, A. Cancer statistics, 2022. *CA Cancer J. Clin.* **72**, 7–33 (2022).
5. Okuda, J. et al. Persistent overexpression of phosphoglycerate mutase, a glycolytic enzyme, modifies energy metabolism and reduces stress resistance of heart in mice. *PLoS One* **8**, e72173 (2013).
6. Li, C. et al. Eicosapentaenoic acid-mediated activation of PGAM2 regulates skeletal muscle growth and development via the PI3K/AKT pathway. *Int. J. Biol. Macromol.* **268**, 131547 (2024).
7. Mikawa, T. et al. Phosphoglycerate Mutase Cooperates with Chk1 Kinase to Regulate Glycolysis. *iScience* **23**, 101306 (2020).
8. Li, Z. et al. Targeting the Metabolic Enzyme PGAM2 Overcomes Enzalutamide Resistance in Castration-Resistant Prostate Cancer by Inhibiting BCL2 Signaling. *Cancer Res.* **83**, 3753–3766 (2023).
9. Sarathi, A. & Palaniappan, A. Novel significant stage-specific differentially expressed genes in hepatocellular carcinoma. *BMC Cancer* **19**, 663 (2019).
10. Li, Y. R. et al. Evaluation of nuclear PGAM2 value in hepatocellular carcinoma prognosis. *Anticancer Drugs* **33**, e500–e506 (2022).
11. Wang, T. et al. Acetylation of lactate dehydrogenase B drives NAFLD progression by impairing lactate clearance. *J. Hepatol.* **74**, 1038–1052 (2021).
12. Deng, Y. et al. HDAC6-dependent deacetylation of AKAP12 dictates its ubiquitination and promotes colon cancer metastasis. *Cancer Lett.* **549**, 215911 (2022).
13. Zhang, S. et al. Hippo Signaling Suppresses Cell Ploidy and Tumorigenesis through Skp2. *Cancer Cell* **31**, 669–684.e667 (2017).
14. Zhang, X. L. et al. K235 acetylation couples with PSPC1 to regulate the m(6)A demethylation activity of ALKBH5 and tumorigenesis. *Nat. Commun.* **14**, 3815 (2023).
15. Zhao, Q. et al. Lysine Acetylome Study of Human Hepatocellular Carcinoma Tissues for Biomarkers and Therapeutic Targets Discovery. *Front. Genet.* **11**, 572663 (2020).
16. Tsusaka, T. et al. Deacetylation of phosphoglycerate mutase in its distinct central region by SIRT2 down-regulates its enzymatic activity. *Genes Cells* **19**, 766–777 (2014).
17. Xu, Y. et al. Oxidative stress activates SIRT2 to deacetylate and stimulate phosphoglycerate mutase. *Cancer Res.* **74**, 3630–3642 (2014).
18. Mikawa, T. et al. Senescence-inducing stress promotes proteolysis of phosphoglycerate mutase via ubiquitin ligase Mdm2. *J. Cell Biol.* **204**, 729–745 (2014).
19. Zhang, Y., Beketaev, I., Ma, Y. & Wang, J. Sumoylation-deficient phosphoglycerate mutase 2 impairs myogenic differentiation. *Front. Cell Dev. Biol.* **10**, 1052363 (2022).
20. Wisniewski, J. et al. High-Resolution Crystal Structure of Muscle Phosphoglycerate Mutase Provides Insight into Its Nuclear Import and Role. *Int. J. Mol. Sci.* **23**, 13198 (2022).
21. Jiang, X., Sun, Q., Li, H., Li, K. & Ren, X. The role of phosphoglycerate mutase 1 in tumor aerobic glycolysis and its potential therapeutic implications. *Int. J. Cancer* **135**, 1991–1996 (2014).
22. Ceballos, M. P., Quiroga, A. D. & Palma, N. F. Role of sirtuins in hepatocellular carcinoma progression and multidrug resistance: Mechanistical and pharmacological perspectives. *Biochem. Pharm.* **212**, 115573 (2023).
23. Ceballos, M. P. et al. Sirtuin 1 and 2 inhibitors enhance the inhibitory effect of sorafenib in hepatocellular carcinoma cells. *Eur. J. Pharm.* **892**, 173736 (2021).
24. Ceballos, M. P. et al. Inhibition of sirtuins 1 and 2 impairs cell survival and migration and modulates the expression of P-glycoprotein and MRP3 in hepatocellular carcinoma cell lines. *Toxicol. Lett.* **289**, 63–74 (2018).
25. Chen, J. et al. SIRT2 overexpression in hepatocellular carcinoma mediates epithelial to mesenchymal transition by protein kinase B/glycogen synthase kinase-3β/β-catenin signaling. *Hepatology* **57**, 2287–2298 (2013).
26. Mei, Z. et al. Sirtuins in metabolism, DNA repair and cancer. *J. Exp. Clin. Cancer Res.* **35**, 182 (2016).
27. Le, A. et al. Inhibition of lactate dehydrogenase A induces oxidative stress and inhibits tumor progression. *Proc. Natl Acad. Sci. USA* **107**, 2037–2042 (2010).
28. Sheng, S. L. et al. Knockdown of lactate dehydrogenase A suppresses tumor growth and metastasis of human hepatocellular carcinoma. *FEBS J.* **279**, 3898–3910 (2012).
29. Aigner, P., Just, V. & Stoiber, D. STAT3 isoforms: Alternative fates in cancer? *Cytokine* **118**, 27–34 (2019).
30. Liang, C., Xu, Y., Ge, H., Li, G. & Wu, J. Clinicopathological significance and prognostic role of p-STAT3 in patients with hepatocellular carcinoma. *Oncol. Targets Ther.* **11**, 1203–1214 (2018).
31. Lee, H., Jeong, A. J. & Ye, S. K. Highlighted STAT3 as a potential drug target for cancer therapy. *BMB Rep.* **52**, 415–423 (2019).
32. Cheng, H. et al. PLCε promotes urinary bladder cancer cells proliferation through STAT3/LDHA pathway-mediated glycolysis. *Oncol. Rep.* **41**, 2844–2854 (2019).
33. Yang, Y. et al. Cryptotanshinone suppresses cell proliferation and glucose metabolism via STAT3/SIRT3 signaling pathway in ovarian cancer cells. *Cancer Med.* **7**, 4610–4618 (2018).
34. Livak, K. J. & Schmittgen, T. D. Analysis of relative gene expression data using real-time quantitative PCR and the 2(-Delta Delta C(T)) Method. *Methods* **25**, 402–408 (2001).

Acknowledgements

We appreciate the continuous support of Henan Key Laboratory for Pharmacology of Liver Diseases where most of the experiments were performed. We thank Youmei Peng for providing the sorafenib resistant HepG2 cell line. This study was supported by the Key Scientific Research Project for Higher Education Institutions in Henan Province (No.

25B320003), the Key Scientific and Technological Project of Henan Province (No. 252102310154, No. 252102310300), and the Project of Basic Research Fund of Henan Institute of Medical and Pharmacological Sciences (No. 2023BP0206, No. 2025BP0101).

Author contributions

W.Z.X. and G.Y.Y. conducted the majority of experimental work and data analysis. H.K.F. and H.T.J. performed the sensitivity assay of HCC cell lines to sorafenib and AGK2 in vitro. Q.T. performed molecular docking and analysis of proteins interaction. Z.L.D. performed the dual-luciferase reporter assay. X.F. helped in experiments design. C.M.J. and X.Y.Z. collected human tissue samples. Z.Q.W. and Z.J.T. designed this study and wrote the paper.

Competing interests

The authors declare no competing interests.

Additional information

Supplementary information The online version contains supplementary material available at https://doi.org/10.1038/s41698-025-00930-9.

Correspondence and requests for materials should be addressed to Jintao Zhang or Qianwei Zhao.